Full-Wave Analysis of Planar Surface-Wave Launchers Offering Efficient Surface-Wave Excitation and Guiding Structure Feeding

Symon K. Podilchak [1, 2], *Samir, F. Mahmoud* [3], *Alois P. Freundorfer* [2], *Yahia M. M. Antar* [1, 2]

[1] Royal Military College of Canada, Kingston, Ontario Canada (antar-y@rmc.ca, skp@ieee.org)

[2] Queen's University, Kingston, Ontario Canada (freund@queensu.ca)

[3] Cairo University, Egypt (samirfm2000@yahoo.com)

Abstract

Classic feeding techniques and dielectric slab selection for planar circuits and antenna designs can be challenging at microwave and millimeter-wave frequencies. Substrates can become electrically thick and unwanted surface-wave (SW) field distributions may be excited potentially spoiling device performance. Thus SWs are typically looked upon as an adverse effect causing parasitic radiation and power losses. However, by using an alternative design approach, SWs can actually be utilized to the advantage as a simple an efficient feeding scheme. In particular, by selecting electrically thick substrates with relatively high dielectric constant values, and with the appropriate arrangement of slots within the ground plane, SWs can be efficiently excited. In this work a full-wave analysis is provided in the spectral domain by examining the fields generated by the main slot connected to the feeding transmission line. Numerical results show that there is a broad frequency range which can offer increased TM SW power levels when compared to the radiated space wave power. Applications for these printed SWLs include new quasi-optical planar circuits, leaky-wave antennas, and other guiding structures for operation at microwave and millimeter-wave frequencies.

1. Introduction

Coplanar waveguide (CPW) fed planar surface-wave launchers (SWLs) have been recognized as an efficient means for coupling power into the dominant SW mode of a grounded dielectric slab (GDS). Both bi-directional and uni-directional surface-wave (SW) field excitation can be achieved [1]. In addition, when relatively high dielectric constants are employed ($\varepsilon_r > 10$), and when the substrate is selected according to $d\sqrt{\varepsilon_r - 1}/\lambda_0 \approx 0.4$, where d is the thickness of the slab and λ_0 is the relevant free-space wavelength, more than 80% of the input power can be coupled into the dominant TM_0 SW mode of the slab. In addition, these SWLs are applicable to new power routing distribution networks and leaky-wave antenna (LWA) designs which can offer efficient operation for microwave and millimeter-wave frequencies [1]. Thus these planar SWLs, or slot arrangements (see Fig. 1), can be thought to act as magnetic dipole sources for bound SW generation.

2. Full-Wave Analysis of the Ground Plane Slot

A rigorous derivation of the near-fields excited by such slot sources are examined in this work. This analysis builds on the findings in [2] where a different approach was theoretically investigated, mainly, the SW fields and the associated powers that can be contained to the slab as a result of an incident plane-wave from the far-field.

Similar results and SW power values are obtained in this work, when compared to [2], however, the two approaches are different. In particular, the near-fields excited by a slot (driven by a feedline) are examined in detail here, versus the derivation using the transverse spectral field representation. However, some basic assumptions are in order at this stage for our near-field approach. One can assume that the bi-directional SWL is a small slot in the ground plane of a lossless GDS and oriented along the y-axis as shown in Fig. 1. Moreover, the main slot is excited by an x-directed electric field, E_x, which originates from the fields generated by the TEM mode on the CPW transmission line (see Fig. 1). It should also be mentioned that an E_z field is also excited within the slab, but the E_x term within the slot is the primary source, which is equivalent to a magnetic current M_y for SW generation. We also consider that this CPW feeding transmission line comes from the periphery of a very large dielectric substrate. Therefore the dimensions of the GDS are significantly larger than the size of the operating free-space wavelength, λ_0. Given these ideal considerations and assumptions, the slot for SW excitation can be considered as a y-oriented magnetic dipole which is also assumed to be positioned at the origin and in the ground

978-1-4673-5225-3/14/$31.00

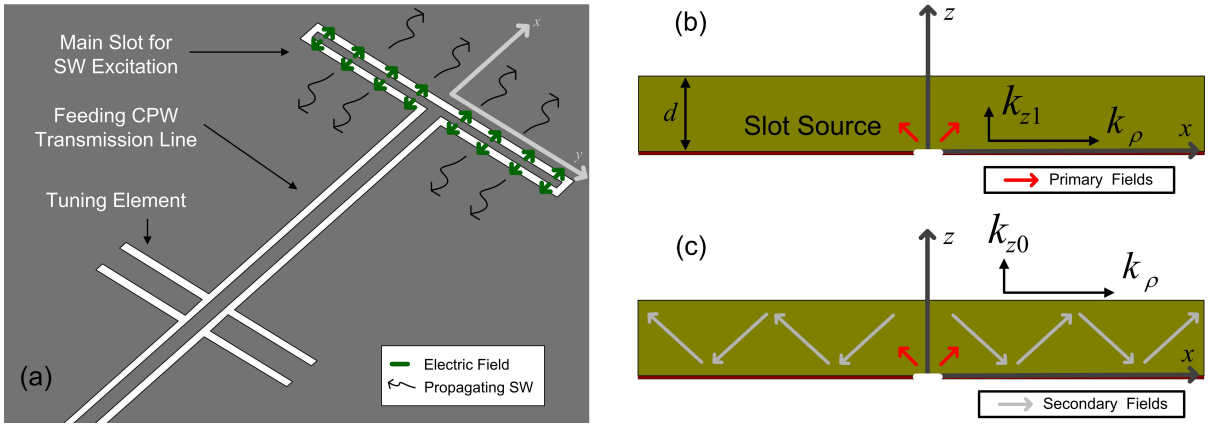

Figure 1: (a): Illustration describing the field coupling from the feeding transmission line and the generated SWs for the bi-directional SWL. The CPW feeding transmission line and the tuning elements for improved matching are shown as well as the main driven slot in the ground plane. (b): The y-oriented slot (with moment K positioned at $z = h = 0$ and $x = 0$) can excite primary waves with both TM and TE field configurations. (c): Due to the boundary conditions at the air interface of the electrically thick GDS, primary waves can be trapped inside the substrate, generating the observed SWs with a radial wave propagation factor.

plane. The variable K (in Volt·m) defines the magnetic moment of this slot source. Following these definitions the generated near-fields can be derived in closed form and expressed as a continuous and discrete spectrum of the radial wavenumber, k_ρ. This respectively refers to the space waves and the SWs generated by the ground plane slot covered by an electrically thick dielectric slab, i.e. $d\sqrt{\epsilon_r}/\lambda_0 < 1$.

One can start the analysis by obtaining the primary field generated by slot in the ground plane as shown in Fig. 1(b). At this stage, and for generality, the placement of the dipole within the slab (with thickness d) will be positioned at $z = h$ such that $h < d$. The primary fields produced by the y-oriented dipole can be derived in terms of a component of the electric vector potential, mainly, $F_y = Ke^{-jk_1R}/4\pi R$ where $R = \sqrt{\rho^2 + (z-h)^2}$ and $k_\rho^2 + k_{z1}^2 = k_1^2 \equiv \omega^2\mu_0\epsilon_0\epsilon_r$ with ρ defining the radial distance from the origin. This component, F_y, can also be represented in integral form using a spectral cylindrical-wave expansion:

$$F_y = \frac{K}{4\pi}\int_0^\infty J_0(k_\rho\rho)e^{-jk_{z1}|z-h|}\, k_\rho/jk_{z1}\;\; dk_\rho \tag{1}$$

where J_0 is the Bessel function of the first kind (order 0) and the time dependent terms ($e^{+j\omega t}$) are suppressed here and throughout.

In Eq. (1) the integration from 0 to k_0 refers to the electric vector potential that will generate a space wave with radiation into the far-field while the integration from k_0 to ∞ is representative of a bound SW [3]. Fields within the slab and air regions are completely obtainable from the E_z and H_z field components. In particular, the electric field can be obtained from Eq. (1) by the relation [4]:

$$\vec{E} = \hat{x}E_x + \hat{y}E_y + \hat{z}E_z = -\nabla \times F_y\hat{y} = +\hat{x}\frac{\partial F_y}{\partial z} - \hat{z}\frac{\partial F_y}{\partial x}\,. \tag{2}$$

However, since the dipole is positioned near the ground plane, the E_x term will vanish in the limit when $h = 0$, defining $\partial F_y/\partial z = 0$. Furthermore, E_y reduces to zero due to the curl operation. These simplifications for the primary field, E_{zp}, are a result of Maxwell's equations, vector operation, and the application of the boundary conditions that exist at the dielectric-conductor interface, mainly that, the tangential electric fields must vanish; i.e. $E_x = 0$. This results in the z-component of the primary electric field to be dominant with $E_{zp} = -\partial F_y/\partial x$. Likewise for the magnetic field

$$\vec{H} = \hat{x}H_x + \hat{y}H_y + \hat{z}H_z = \nabla \times \nabla \times F_y\hat{y}\,/\,j\omega\mu_0 = -\nabla \times \vec{E}\,/\,j\omega\mu_0 \tag{3}$$

and with $j\omega\mu_0 H_{zp} = \partial^2 F_y/\partial y\partial z$ [4]. Of particular interest is the phase propagation factor, $e^{-jk_{z1}|z-h|}$, which defines field propagation for the primary TM and TE field terms, E_{zp} and H_{zp}, respectively. In addition, these

wave parts can be treated separately since they are uncoupled at the air-dielectric interface. Thus, these primary TM and TE fields can be further established:

$$E_{zp} = -\frac{\partial F_y}{\partial x} = jK\frac{1}{4\pi}\frac{\partial}{\partial x}\int_0^\infty J_0(k_\rho\rho)e^{-jk_{z1}|z-h|}\, k_\rho/k_{z1}\;\, dk_\rho \tag{4}$$

and

$$H_{zp} = \frac{1}{j\omega\mu_0}\frac{\partial^2 F_y}{\partial y \partial z} = -jK\frac{1}{4\pi\omega\mu_0}\frac{\partial}{\partial y}\int_0^\infty J_0(k_\rho\rho)e^{-jk_{z1}|z-h|}\, k_\rho\;\, dk_\rho\,. \tag{5}$$

The total fields in the slab can now be expressed in terms of the primary fields, E_{zp} and H_{zp}, and the secondary fields which are a result of reflections at the ground plane and the air-dielectric interface at $z = d$. This is illustrated in Fig. 1(b), and given this full-wave analysis approach, the total TM and TE fields within the slab can be further established:

$$E_z = j\frac{K}{4\pi}\frac{\partial}{\partial x}\int_0^\infty J_0(k_\rho\rho)\, f(k_\rho; z)\, k_\rho/k_{z1}\;\, dk_\rho$$

and

$$H_z = j\frac{K}{4\pi\omega\mu_0}\frac{\partial}{\partial y}\int_0^\infty J_0(k_\rho\rho)\, g(k_\rho; z)\, k_\rho\;\, dk_\rho\,. \tag{6}$$

In Eq. (6) the spectral functions $f(k_\rho; z)$ and $g(k_\rho; z)$ characterize the total fields within the slab and are determined by applying boundary conditions [3]. In addition, the poles of $f(k_\rho; z)$ and $g(k_\rho; z)$ respectively define the TM and TE SW modes of the GDS.

In the air region and above the dielectric ($z > d$), expressions for the TM and TE fields are as follows:

$$E_z = j\frac{K}{4\pi}\frac{\partial}{\partial x}\int_0^\infty J_0(k_\rho\rho)\, f_{air}(k_\rho; z)\, e^{-jk_{z0}(z-d)}\, k_\rho/k_{z1}\;\, dk_\rho$$

and

$$H_z = j\frac{K}{4\pi\omega\mu_0}\frac{\partial}{\partial y}\int_0^\infty J_0(k_\rho\rho)\, g_{air}(k_\rho; z)\, e^{-jk_{z0}(z-d)}\, k_\rho\;\, dk_\rho \tag{7}$$

where $k_{z0}^2 = k_0^2 - k_\rho^2$ and $k_0^2 = \omega^2\mu_0\epsilon_0$. By the application of the boundary conditions that exist at the air-dielectric interface, the spectral functions $f(k_\rho; z)$, $g(k_\rho; z)$, $f_{air}(k_\rho; z)$, and $g_{air}(k_\rho; z)$ can be determined in closed form. In particular, by applying the continuity of εE_z and $\partial E_z/\partial z$ for the TM part, and analogously, the continuity of the H_z and $\partial H_z/\partial z$ terms for TE waves.

The amount of SW power launched from the slot into single layer slab as well, as the radiated power, can be further characterized. For example, one can define the input power, P^{in}, as the total power delivered by the SW source. Since the slot is positioned at the origin (defined here as $\rho = 0$ and $z = 0$), the real input power must be equal to the sum of the radiated power and the power launched into the SW modes. This is given by

$$P^{in} = -K\,\Re e\left\{H_y(\rho = 0, z = 0)\right\} = P^{Rad} + P^{SW} = P^{Rad} + P_{TM}^{SW} + P_{TE}^{SW} \tag{8}$$

since the units for the the magnetic moment, K, of this slot source is Volt·m while the units for H_y are Amps/m. Also notice that a distinction is made between the TM and TE SW powers in that the total SW power is the addition of the TM and TE SW powers; i.e. $P^{SW} = P_{TM}^{SW} + P_{TE}^{SW}$. Here the H_y term in Eq. (8) describes the magnetic field in the dielectric region and can be obtained from Eq. (6).

Calculated radiated powers along with the relative SW powers are shown in Fig. 2 for the substrate parameters ($\varepsilon_{r1} = 10.2$, $h = 1.27$ mm) which have been shown to offer efficient SW excitation [1], [2]. Results show that the total SW power can approach 90% when compared to the input power. These values are consistent with the numerical results obtained in [2] where the SW powers were examined using the transverse spectral field representation (see Figs. 2 and 8 from [2]). Moreover, in both analyses maximum SW coupling efficiencies can occur after the TE_1 SW mode cutoff frequency of the slab. It should also be mentioned that for the investigated frequency band, from 10 to 35 GHz as shown in Fig. 2, only the TM_0 and the TE_1 modes exist. This investigation could also be extended beyond 35 GHz, however, higher order SW modes would need to be considered.

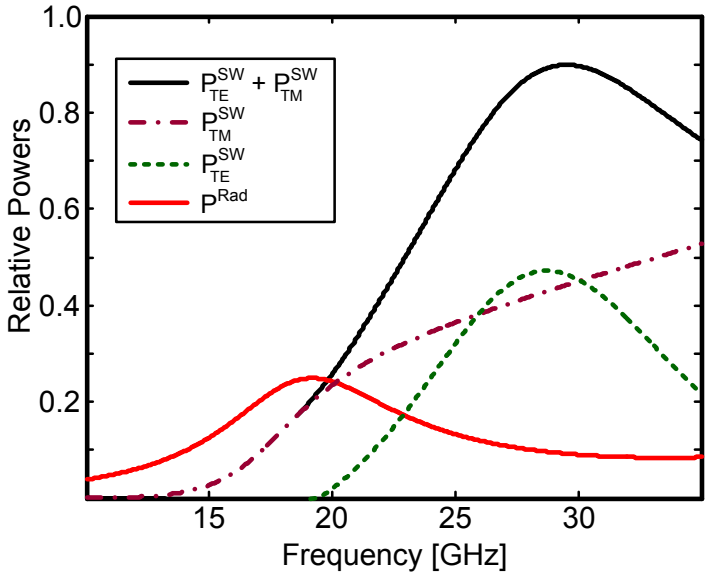

Figure 2: Increased SW power levels can be observed after the TE_1 cutoff frequency of the slab (no material losses considered), when compared to P^{in}, with values approaching 90%.

An important design consideration for the investigated SWLs is an estimation of the amount of SW power relative to the power radiated into the far-field. A measure of this comparison (or percentage SW power) can be defined as the SWL efficiency:

$$\eta^{SWL} \propto \frac{P^{SW}}{P^{Rad} + P^{SW}}. \tag{9}$$

This ratio is defined as the amount of SW power coupled into the SW modes compared to the total input power. Given the results of Fig. 2 the desired frequency of operation of the SWL should occur where the radiated power is minimal with the SW power obtaining maximum values. This is shown to occur after the TE_1 SW mode cutoff frequency of the slab (19.47 GHz), at about 23 GHz or $h\sqrt{\epsilon_r}/\lambda_0 \approx 1/4$. In addition, the radiated space power also decreases in this range (at about 23 GHz) but with increased power levels in the TE fields.

3. Conclusion

The surface-waves (SWs) excited by a bi-directional surface-wave launcher (SWL) have been examined. In particular, slotted configurations in the ground plane of a dielectric slab can act as a SW source and this planar SWL design is fed by a coplanar waveguide transmission line allowing for simple integration with other planar devices at microwave and millimeter-wave frequencies. Essentially, the input signal is coupled into the dominant TM_0 SW mode of the slab. More importantly, efficient field confinement can be realized offering a simple technique for SW control [1]. These practical feeding concepts can also be applied to new and innovative SW-fed devices for communication applications which can outperform more conventional designs that attempt to suppress the fundamental TM_0 SW mode.

4. References

1. S. K. Podilchak, "Planar Leaky-Wave Antennas and Microwave Circuits by Practical Surface Wave Launching," *Ph.D. Dissertation*, Queen's University, Kingston, Ontario, Canada, Sept. 2013.

2. S. Mahmoud, Y.M.M. Antar, H. Hammad, and A. Freundorfer, "Theoretical Considerations in the Optimization of Surface Waves on a Planar Structure," *IEEE Trans. Ant. Prop.*, vol. 52, no. 8, pp. 2057–2063, Apr. 2004.

3 S. F. Mahmoud and Y. M. M. Antar, *Microstrip and Printed Antennas: New Trends, Techniques and Applications, Ch. 13*, Hoboken, New Jersey: Wiley, 2011.

4. R. F. Harrington, *Time-Harmonic Electromagnetic Fields*, New Jersey, USA: Wiley Press, 2001.